Atomic layer deposition of hafnium oxide from *tert*-butoxytris(ethylmethylamido)hafnium and ozone: rapid growth, high density and thermal stability

Minha Seo,[a] Yo-Sep Min,[b] Seong Keun Kim,[a] Tae Joo Park,[a] Jeong Hwan Kim,[a] Kwang Duk Na[a] and Cheol Seong Hwang*[a]

Received 15th April 2008, Accepted 7th July 2008
First published as an Advance Article on the web 4th August 2008
DOI: 10.1039/b806382f

HfO_2 thin films were grown by atomic layer deposition (ALD) using a novel heteroleptic precursor, *tert*-butoxytris(ethylmethylamido)hafnium [$HfO^tBu(NEtMe)_3$; BTEMAH] and ozone. The structure of BTEMAH is similar to that of tetrakis(ethylmethylamido)hafnium [$Hf(NEtMe)_4$; TEMAH] except that one of its four amido ligands is replaced with a *tert*-butoxy ligand. This heteroleptic structure largely improves the ALD growth rate (0.16 nm cycle^{-1}) and Hf density (Hf mass per unit volume of HfO_2 film, 7.6 g cm^{-3}) of the HfO_2 films. The self-regulated ALD growth behavior was confirmed at a growth temperature of 300 °C. Higher Hf density induces anti-crystallization properties in the as-grown film. Consequently, the amorphous phase of a HfO_2 film is retained up to ~15 nm during deposition at 300 °C. The more amorphous-like nature and the higher Hf density of the HfO_2 film also retard crystallization during post-deposition annealing (PDA), which strongly enhances the thermal stability of the electrical performance. The capacitance equivalent thickness of the films with thicknesses ranging from 4 to 13 nm is relatively constant up to a PDA temperature of 1000 °C.

Introduction

Atomic layer deposition (ALD) is considered to be a promising method for growing various thin films, including oxides, nitrides, and metals, on account of its excellent thickness control, uniform growth over large areas, conformal growth on three dimensional structures and relatively low growth temperature compared with chemical vapor deposition (CVD).[1–3] In ALD, the metal precursor and reactant molecules are alternately pulsed to a reactor at low temperatures in order to avoid thermal decomposition. Between the two pulses, an inert gas is supplied to purge the excess amount of precursor and reactant. Therefore, the growth rate of ALD is not accelerated by increasing the doses of the precursor and reactant, and is rather self-limited by chemisorption. However, the generally low growth rate (film thickness increase per cycle, typically lower than ~0.1 nm cycle^{-1}) of ALD restricts its application to thinner films in the fabrication of semiconductor devices.

Recently, ALD of HfO_2 has been studied extensively as a possible replacement for the gate oxide (SiO_2) in field effect transistors (FETs) owing to its high dielectric constant and thermal stability on silicon surface.[4–11] The most frequently investigated precursors for ALD of HfO_2 are hafnium tetrachloride ($HfCl_4$),[5–7] tetrakis(*tert*-butoxy)hafnium [$Hf(O^tBu)_4$][8] or tetrakis(alkylamido)hafnium [$Hf(NR_1R_2)_4$].[9–11] The growth rate of HfO_2 films from $HfCl_4$ and H_2O is only ~0.05 nm cycle^{-1} at 300 °C.[5–7] $Hf(O^tBu)_4$ is vulnerable to easy thermal decomposition, which precludes the proper operation of a self-limiting mechanism.[8] The use of tetrakis(alkylamido)hafnium precursors with water or ozone generally increases the growth rate of HfO_2 up to almost 0.1 nm cycle^{-1}.[9–11] The vapor pressures for tetrakis(diethylamido)hafnium (TDEAH; $R_1 = R_2 =$ Et), tetrakis(ethylmethylamido)hafnium (TEMAH; $R_1 =$ Et, $R_2 =$ Me), and tetrakis(dimethylamido)hafnium (TDMAH; $R_1 = R_2 =$ Me) at 70 °C are 0.04, 0.3 and 1.9 Torr, respectively.[12] Although the growth rate of HfO_2 using these precursors is double that of $HfCl_4$, it is still unsatisfactorily low. A cyclopentadienyl Hf precursor can be used for ALD of HfO_2 up to 500 °C without thermal decomposition but its growth rate is still approximately 0.05 nm cycle^{-1}.[13]

The other problem with HfO_2 as a high-*k* gate dielectric film grown by ALD is crystallization during deposition when the film thickness is greater than ~5 nm for processes using $HfCl_4$ and H_2O (ref. 5) and greater than ~8 nm for TDMAH and H_2O.[14] Crystallized high-*k* gate dielectric films generally have inferior leakage current, reliability, carrier mobility in the channels and thermal stability during post-deposition annealing (PDA) to those of amorphous high-*k* films. The low growth temperature of ALD processes (less than ~300 °C) generally produces amorphous films during deposition when the films are thinner. As the film becomes thicker with increasing number of deposition cycles, crystalization is driven by the higher bulk free energy of the amorphous materials compared with that of the crystalline material. In the case of a thin film under a critical thickness (the thickness where the transition from amorphous to crystalline occurs), the decrease in bulk free energy by crystallization cannot compensate for the increase in free energy due to the formation of grain boundaries and the interface between amorphous and

[a]*Department of Materials Science and Engineering, Inter-university Semiconductor Research Center, Seoul National University, Seoul, 151-744, Korea. E-mail: cheolsh@snu.ac.kr; Fax: +82 2 884 1413; Tel: +82 2 880 7535*
[b]*School of Chemical & Biological Engineering, Konkuk University, Seoul, 143-701, Korea*

crystalline layers. The easier crystallization is believed to be due to the relatively low density of the films compared with the bulk material. Therefore, it is highly desirable to have an ALD process for growing HfO_2 films with a higher growth rate and with anti-crystallization properties. It is believed that obtaining a high Hf density (Hf mass per unit volume of HfO_2 film) of the film is beneficial for achieving anti-crystallization properties.

It was previously reported that O_3 is generally a better reactant than H_2O for the ALD of HfO_2 films for both $HfCl_4$ and organometallic precursor (TDMAH).[15,16] However, the growth rate is still low and the films easily crystallize during ALD and PDA. In this study, a new heteroleptic hafnium precursor, *tert*-butoxytris(ethylmethylamido)hafnium (BTEMAH),[17] was used in combination with O_3 to achieve a high growth rate and anti-crystallization behavior. Heteroleptic hafnium precursors combining *tert*-butoxy with the other ligands, such as 2-(4,4-dimethyloxazolinyl)propanolate (dmop) or 1-methoxy-2-methyl-2-propanolate (mmp), are much more stable in air and moisture than $Hf(O^tBu)_4$.[18,19]

BTEMAH is a heteroleptic complex of hafnium with one *tert*-butoxy and three ethylmethylamido ligands. Its volatility is intermediate between $Hf(O^tBu)_4$ and TEMAH, and it shows higher reactivity than TEMAH due to the presence of the *tert*-butoxy ligand.[17] It was expected that replacing one of the ethylmethylamido ligands with a highly reactive *tert*-butoxy ligand would improve the growth behavior and properties of HfO_2 films. In this study, the growth rate of HfO_2 from BTEMAH was $\sim$0.16 nm cycle^{-1} at a growth temperature of 300 °C, which is the highest value for ALD HfO_2 reported thus far. The Hf density of the film was also improved. The anti-crystallization behavior was enhanced due to the high Hf density of the as-grown films. For comparison, the ALD behavior of HfO_2 films using the TDMAH precursor was also examined using the same ALD reactor under otherwise similar conditions.

Experimental procedure

HfO_2 films were deposited on p-type 4 inch diameter (100) Si wafers using a traveling-wave type ALD reactor (Quros Co, Plus-100) with BTEMAH and ozone as the hafnium precursor and oxidant, respectively. Prior to deposition, the wafers were cleaned with standard RCA cleaning and dipping into a dilute HF solution ($HF : H_2O = 1 : 10$). Ozone was produced using an induction-type ozone generator (Astex, AX8200) where an O_2–N_2 gas mixture was introduced and its concentration was controlled from 150 g m^{-3} to 400 g m^{-3} by changing the voltages applied to the ozone generator. An ozone concentration of 330 g m^{-3}, which was measured using an ozone concentration monitor (AFX, model H1-X), was used in all experiments. Although Park *et al.*[20] and Kamiyama *et al.*[21] reported the influence of the ozone concentration on the growth behavior and film properties in the case of using TDMAH and TEMAH precursor, respectively, only the results with a fixed ozone concentration are reported in this study for clarity. The BTEMAH precursor was kept at 45 °C, where a vapor pressure of 0.1 Torr was achieved, and carried by 200 standard cubic centimeters per minute (sccm) of Ar carrier gas. An Ar pulse of 800 sccm was used after the BTEMAH and ozone pulses to remove the volatile byproducts and any excess reactants for 5 s and 3 s, respectively. The BTEMAH precursor was purchased from Asahi-denka Kyogo, Japan. The BTEMAH and ozone injection times were varied in order to check the saturated growth behavior. The deposition temperature was varied from 250 to 350 °C, and the working pressure was $\sim$1 Torr. For comparison, the HfO_2 films were deposited using TDMAH and ozone. The HfO_2 films using the TDMAH precursor were deposited under the same conditions as the HfO_2 films using the BTEMAH precursor but the precursor injection time was fixed to 0.5 s, which was previously determined to be the proper ALD condition.[16] The growth temperature of 300 °C was certainly within the ALD process temperature window for TDMAH. The thermal stability of the films was estimated by performing PDA under a N_2 atmosphere using rapid thermal annealing (RTA) at temperatures ranging from 500 °C to 1000 °C for 1 min.

All the film thickness data in this study, except for the data shown in Fig. 6, 7 and 10, were obtained using a spectroscopic ellipsometer (J. A. Woolam, EC-400). The incident angle of the spectroscopic ellipsometer was fixed at 75° and the data were fitted using a Cauchy dispersion function. The model structure is 'Cauchy (x nm)/Si'. Therefore, every reported thickness using a spectroscopic ellipsometer in this paper includes the interfacial layer between the HfO_2 film and Si substrate. The thickness data shown in Fig. 6 and 10 were measured from high-resolution transmission electron microscopy (HRTEM, JEOL, 3000F) images. In the HRTEM images, interfacial layer thickness was measured from the end of the Si lattice image to the boundary of the gray contrast between the interfacial layer and upper layer. The upper layer thickness was measured from that boundary to the end of the upper layer image. The thickness of every layer in HRTEM was calculated in reference to the Si substrate (111) lattice fringe in each image, which is 3.135 Å. The thickness data in Fig. 7 were measured using a single-wavelength ellipsometer (Gaertner, L-116D). The glancing angle X-ray diffraction (GAXRD) measurements were carried out using a Philips X'pert Pro MRD X-ray diffractometer with Cu Kα radiation. The chemical composition and impurity content in the films were examined by Auger electron spectroscopy (AES, VG Scientific Microlab 350). Depth profile using AES was created by sputtering using accelerated Ar^+ ions. HRTEM was used to examine the crystallinity and interfacial layer changes. The Hf density of the films was measured by X-ray fluorescence spectroscopy (XRF, Spectrace, QuanX). The surface morphology of the films was investigated by atomic force microscopy (AFM, JEOL, JSPM5100).

In order to examine the electrical properties of the HfO_2 films, metal–insulator–semiconductor (MIS) capacitors were fabricated by depositing 100 nm-thick Pt films using an electron beam evaporator through a metal shadow mask for the top electrodes. The area of the Pt electrode was approximately 6.0×10^4 μm^2, and the accurate area of each measured capacitor was acquired by optical microscopy. Forming gas (5% H_2–95% N_2 mixture gas) annealing was performed at 400 °C after top electrode deposition. A Hewlett-Packard 4194A impedance analyzer and a 4140B picoammeter were used for the capacitance–voltage (C–V) and current density–voltage (J–V) measurements, respectively. Five to ten capacitors were measured from each sample to compensate for local variations. The C–V measurement frequency was 1 MHz.

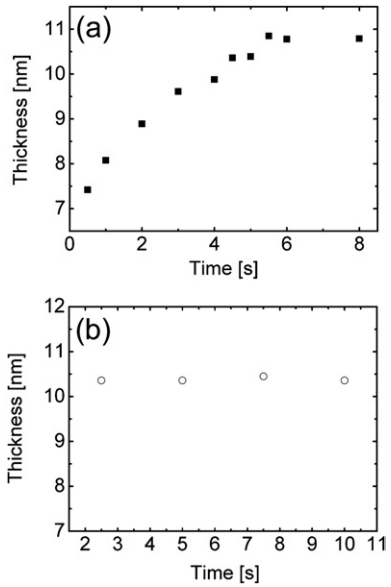

Fig. 1 (a) Changes in thickness in 50 cycle-deposited HfO_2 films at a deposition temperature of 300 °C as a function of the BTEMAH precursor injection time with a fixed purge time of 5 s. (b) Changes in film thickness as a function of the Ar purge time with a fixed precursor injection time of 4.5 s. The time shown on the *x*-axis corresponds to the source feeding (a) or purge (b) time.

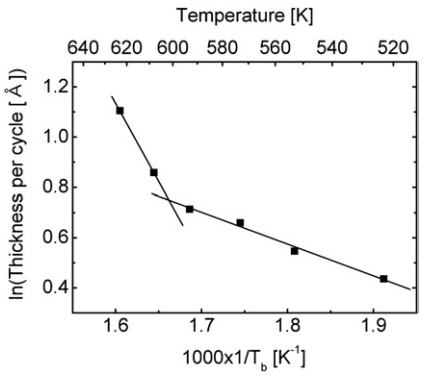

Fig. 2 An Arrhenius plot showing the growth temperature dependence of 50 cycle-deposited HfO_2 film thickness using BTEMAH.

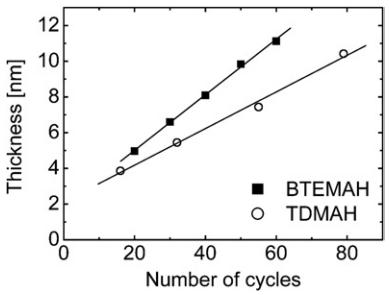

Fig. 3 The changes in the thicknesses of HfO_2 films using BTEMAH and TDMAH grown at 300 °C measured by spectroscopic ellipsometer as a function of number of cycles.

Results and discussion

Growth and crystallization behavior

Fig. 1(a) shows HfO_2 films deposited at 300 °C for 50 cycles with various BTEMAH pulse times to confirm the self-limiting growth mechanism of ALD. In this study, the ozone pulse and the purge times of BTEMAH and ozone were fixed at 3, 5, and 3 s, respectively. Fig. 1 shows that the film thickness increases with increasing the BTEMAH pulse up to 5.5 s, and then saturates near 10.8 nm. This suggests that film growth is self-limited under these conditions. When the film thickness was saturated, the thickness non-uniformity [(maximum thickness − minimum thickness)/2 mean thickness] of the film over a 4 inch wafer decreased significantly from 25% to 2%. This also confirms that a stable ALD process window was obtained. Fig. 1(b) shows the film thickness (50 cycles) as a function of the BTEMAH purge time with a BTEMAH pulse time of 4.5 s. There is almost no decrease in thickness at purge times ranging from 2.5 to 10 s, which suggests that a purge time of 2.5 s is long enough to remove any excess BTEMAH and byproduct molecules. A purge time of 5 s was used in this study to guarantee sufficient purging. However, the ALD cycle time can be further shortened in a well-established reactor for mass production. Although the self-limiting growth behavior along the ozone pulse is not shown, an ozone pulse of 3 s is considered long enough for ALD with the ozone concentration of 330 g m^{-3}.

Fig. 2 shows the growth temperature dependence of the HfO_2 films in Arrhenius form. The natural logarithm of the growth rate of HfO_2 films increased linearly with decreasing reciprocal growth temperature (in Kelvin) up to 320 °C. The calculated apparent activation energy from the slope was 10.6 kJ mol^{-1}. At temperatures ranging from 335 to 350 °C, the apparent activation energy was 51.8 kJ mol^{-1}, which is possibly due to the thermal decomposition of the whole BTEMAH molecule.[22,23] A growth temperature <320 °C corresponds to the ALD window considering the self-limiting growth behavior at 300 °C shown in Fig. 1.

Fig. 3 shows the HfO_2 film thickness variation as a function of the number of cycles at a growth temperature of 300 °C. The ALD growth rate was estimated to be 0.16 nm $cycle^{-1}$ from the slope in Fig. 3. The growth rate of 0.16 nm $cycle^{-1}$ at 300 °C is the highest value reported thus far. The reported growth rates of HfO_2 films by ALD are not much higher than 0.1 nm $cycle^{-1}$.[9] This is a crucial merit of this precursor for mass production compared with the others. Also shown in Fig. 3 is the change in film thickness using the TDMAH and O_3 under similar conditions as a function of the number of cycles at the same growth temperature. The calculated growth rate was 0.10 nm $cycle^{-1}$.

Fig. 4 shows the AES depth profile of the HfO_2 film grown at 300 °C from BTEMAH and ozone. The carbon and hydrogen concentrations are not shown in Fig. 4 because they were below the background noise level. The Si concentration inside the HfO_2 film was also less than ~1%. This suggests that the high growth rate of HfO_2 from BTEMAH is not due to impurities in the film.

The growth rate estimated from the film thickness is generally correlated with the density of the grown film. Fig. 5 shows the Hf areal density (D_A) variations in the HfO_2 films as a function of the film thickness (t). XRF here cannot detect oxygen. The Hf

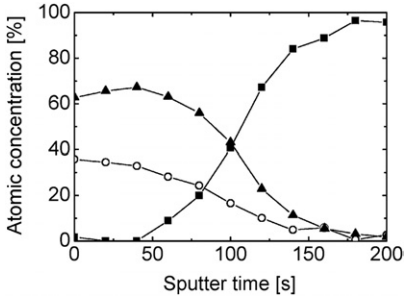

Fig. 4 AES depth profiles of Si, Hf, O of 50 cycle-deposited HfO_2 film using BTEMAH precursor at a deposition temperature of 300 °C. The closed squares, closed triangles, and open circles correspond to Si, O, and Hf, respectively.

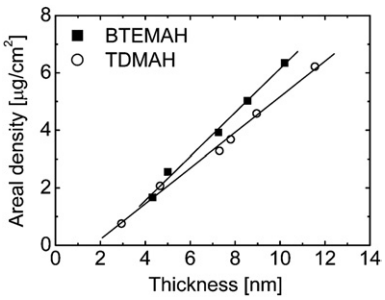

Fig. 5 The variations in the Hf areal density of the films using BTEMAH and TDMAH as a function of the film thickness. The slopes give bulk Hf density of each film.

areal densities were obtained with HfO_2 films grown at 300 °C from BTEMAH and TDMAH. The Hf areal density increased linearly with the increasing t (and number of ALD cycles), but the slope depends on the precursor type. It was assumed that the films consist of an upper layer (UL) of HfO_2 and an interfacial layer (IL) between HfO_2 and Si substrate. The volume densities of Hf in the upper layer (d_{UL}) and the average value (d_{av}) in the remaining part of the film (IL and transition region between the UL and IL) were obtained from the slope and y-axis intercept in Fig. 5, respectively, using the simple equation: $D_A = (t - t_{IL} - t_{tr})d_{UL} + (t_{IL} + t_{tr})d_{av}$, where t_{IL}, and t_{tr} are the thickness of the interfacial layer (determined from the y-axis intercept of Fig. 3) and transition layer between the UL and IL, respectively. t_{tr} was assumed to be 0.5 nm. This is because the t_{IL} estimated from the y-axis intercept of Fig. 3 corresponds to the initially grown IL thickness at the early stages of film growth. However, t_{tr} is formed during the subsequent HfO_2 growth step, and this layer must have a different Hf density from those of the UL and IL. d_{UL} was assumed to be independent of the thickness, and d_{av} is a measure of the degree of Hf diffusion into the IL region during film growth.

The calculated Hf densities of the upper layer (d_{UL}) and d_{av} were 7.6 and 1.4 g cm^{-3}, respectively, for BTEMAH, and 6.2 and 2.3 g cm^{-3}, respectively, for TDMAH. It should be noted that the ideal Hf bulk density of HfO_2 was estimated to be 8.21 g cm^{-3} from the ideal HfO_2 density of 9.68 g cm^{-3}.[24] The absolute value is subjected to some degree of error because an arbitrarily assumed value of 0.5 nm was used for t_{tr}. Therefore, only a relative comparison between the two types of samples has relevance. The HfO_2 films from BTEMAH not only have a high thickness growth rate but also a higher Hf density. This means that the high growth rate of HfO_2 films using BTEMAH is not caused by the formation of porous films during deposition. The non-negligible d_{av} values suggest that hafnium atoms diffuse into interface layer that was formed by the oxidation of Si substrate during ALD. A higher d_{av} value for the films grown from TDMAH compared with that from BTEMAH suggests that the diffusion of Hf atoms is more serious, possibly due to the less dense and crystalline structure of HfO_2 layer, as will be shown later. The films grown from BTEMAH were not crystallized over the entire thickness region shown in Fig. 5. The difference in the Hf density of the upper HfO_2 layer and the interfacial layer largely affects the crystallization behavior and dielectric constants, as will be shown later.

Fig. 6(a) shows the GAXRD data of the as-deposited HfO_2 films from BTEMAH at various thicknesses, and a 12.3 nm-thick film after annealing at 900 °C. It is generally accepted that the crystallization of HfO_2 films degrades their electrical properties. Cho *et al.* reported that HfO_2 films grown from $HfCl_4$ and H_2O crystallize when the film thickness is greater than ~5 nm,[5] and the

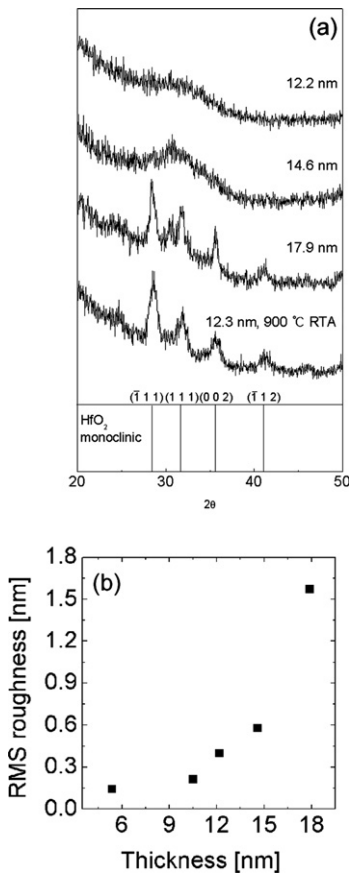

Fig. 6 (a) GAXRD spectra of 12.2, 14.6, 17.9 nm-thick as-deposited HfO_2 films, and 12.3 nm-thick post annealed HfO_2 films (900 °C) using BTEMAH precursor. The peak positions of the HfO_2 monoclinic structure are included at the bottom. (b) Variation in the RMS roughness of the as-deposited HfO_2 films using the BTEMAH precursor as a function of the film thickness.

films from TDMAH and ozone crystallize when its thickness is greater than ~8 nm.[14] Moreover, almost all HfO_2 films using these precursors ($HfCl_4$ and TDMAH) crystallized completely after annealing at temperatures >600 °C. However, there is no crystalline peak in the diffraction patterns in Fig. 6(a) for the as-grown HfO_2 films from BTEMAH even at a thickness of 14.6 nm. The thicker as-grown film (17.9 nm) and film (12.3 nm) annealed at 900 °C crystallize in a monoclinic phase. The observed peaks were assigned to the ($\bar{1}11$), (111), (002) and ($\bar{1}12$) planes of monoclinic HfO_2. Carbon or other impurities in the film have a low concentration, below the AES detection limit (~1 atomic%, Fig. 4). Hence, the suppression of crystallization is not caused by the presence of impurities. However, GAXRD might not be accurate enough to detect crystalline phases in ultra-thin films (<10 nm). Therefore, the crystallization behavior of the films was further confirmed by AFM and wet-etching experiments.

Fig. 6(b) shows the change in the root-mean-square (RMS) roughness of the as-grown films as a function of the thickness obtained by AFM. The result shows that the films maintain a very smooth surface (<0.6 nm) up to a thickness of ~14 nm, which coincides with the critical thickness for crystallization. After crystallization either by increased thickness or annealing, the film morphology becomes granular and the RMS roughness increases abruptly. This agrees well with the GAXRD results.

Wet etching of the films, using an aqueous hydrofluoric acid solution ($HF : H_2O = 1 : 10$), is a good way of testing the crystalline state of the HfO_2 film because crystalline films are barely etched whereas amorphous films are well etched.[25] This property of HfO_2 allows the confirmation of crystalline films, particularly when the film thickness is too thin for the use of standard X-ray diffraction. Fig. 7(a) shows the changes in film thickness as a function of the wet-etching time for the 10.5, 14.6, and 17.9 nm-thick as-grown films, and an annealed film (12.3 nm) at 900 °C. Although the data are not shown here, wet etching of thinner films is very fast. When the film was 10 nm thick, it was etched almost completely within 60 s. The etch rate of the as-grown films decreases with increasing thickness, and finally a certain thickness remains even after prolonged etching. For example, the thickest film (17.9 nm) was etched slowly, and etching was eventually stopped at a thickness of 13.5 nm while the 14.6 nm-thick film was almost completely etched away within ~2 min. The annealed film (12.3 nm) at 900 °C was not etched due to its highly crystalline structure. From the GAXRD, AFM, and etching experimental results, it is believed that as-grown films thinner than ~13 nm are completely amorphous, the ~15 nm-thick film is slightly crystallized, and the ~17 nm-thick film is highly crystalline. Consequently, the critical thickness for as-grown crystallization during ALD is increased to ~15 nm only using BTEMAH due to the high density of as-grown films. The higher density of the film suppresses the migration of constituent ions in the as-deposited film, which is essential for crystallization. It should be noted that the value of the critical thickness is almost triple and double that of the corresponding thickness of HfO_2 films from $HfCl_4$ and TDMAH, respectively.

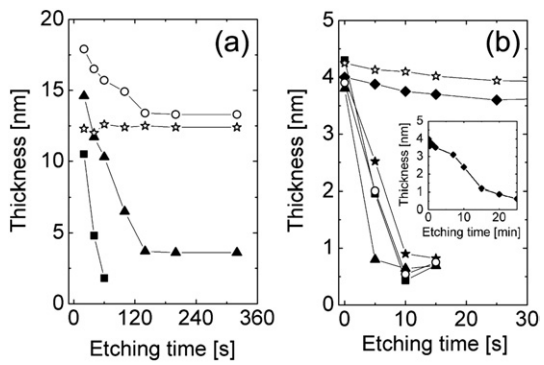

Fig. 7 (a) Changes in the HfO_2 film thickness using BTEMAH as a function of the wet-etching time. The etch rate of 10.5 nm (■), 14.6 nm (▲), and 17.9 nm (○) thick as-deposited HfO_2 films was ~0.22, 0.089, and 0.034 nm s^{-1}, respectively. The 12.3 nm-thick film (☆) was not etched at all after annealing at 900 °C. (b) Changes in the HfO_2 film thickness using BTEMAH as a function of wet-etching time after annealing at 500 °C (▲), 600 °C (○), 700 °C (★), 800 °C (◆) and 900 °C (☆) and the as-deposited film (■). The film annealed at 800 °C was almost completely etched after 15 min (inset).

Fig. 7(b) shows the anti-crystallization property against annealing at high temperatures. As-grown films from BTEMAH, in which initial thicknesses were 4–4.5 nm, were annealed for 1 min at 500, 600, 700, 800, and 900 °C, and wet-etched using the same etching solution. The change in thickness as a function of the wet-etching time shows that the etching rate decreases slightly with increasing annealing temperature up to 700 °C. However, the films are essentially well etched below this temperature. When the annealing temperature was increased above 800 °C, the wet-etching rate decreased abruptly suggesting that the film crystallized at this temperature. Therefore, it is believed that the amorphous phase of the as-grown HfO_2 films is maintained up to an annealing temperature of 700–800 °C. The inset in Fig. 7(b) shows the wet etching test results up to 25 min. The annealed film, even at 800 °C, was almost completely etched away in such a long etching time. The film annealed at 900 °C was not etched away after the same long etching time. This suggests that at least 900 °C is needed for the complete crystallization of films <5 nm in thickness grown from BTEMAH. This is in contrast to the crystallization behavior of HfO_2 films grown from $HfCl_4$ and TDMAH which are well crystallized by annealing even at 700 °C.[14]

The crystallization behavior of HfO_2 films grown from BTEMAH and TDMAH was further confirmed by HRTEM. Fig. 8(a), (b), and (c) show HRTEM images of the as-grown films from BTEMAH and the annealed films at 700 and 1000 °C, respectively, for 1 min, and (d), (e), and (f) show the corresponding images of films grown from TDMAH. The films were composed of two layers (interfacial layer and upper layer) as mentioned above. The interfacial layer is believed to be SiO_{2-x} with a low Hf concentration for the case of BTEMAH or SiO_{2-x} with relatively higher Hf concentration in the case of TDMAH, as shown by the low and high Hf density in these interfacial layers (Fig. 5). It is clearly shown that the upper layers of HfO_2 in both cases are amorphous in the as-grown state. After annealing at 700 °C, the HfO_2 films from BTEMAH still remains in the amorphous structure, whereas the HfO_2 film from TDMAH is totally crystallized at the same temperature. Both films were crystallized by annealing at 1000 °C.

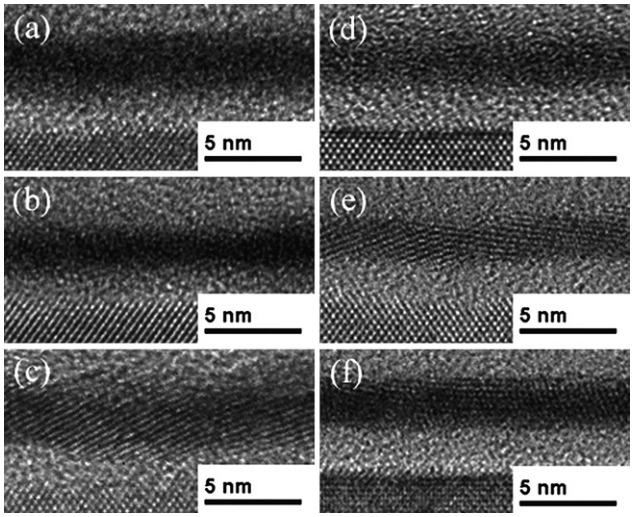

Fig. 8 Cross-section HRTEM images of HfO_2 films using the BTEMAH precursor (a) in the as-grown state (at 300 °C), and after annealing at (b) 700 and (c) 1000 °C. Images (d)–(f) show the corresponding films using TDMAH.

Another notable finding from the HRTEM images is the variation in the thickness of each layer after annealing. During ALD, the interfacial layer grows by oxidation of the Si substrate. When the upper layer with a certain thickness is formed, oxygen atoms should diffuse through the grown upper layer for interfacial layer growth. The interfacial layer thickness in the case of BTEMAH was thinner than that in the case of TDMAH. The interfacial layer thicknesses of the as-deposited films, and films after PDA at 700 and 1000 °C in the case of the BTEMAH precursor, were 1.1 ± 0.1, 0.8 ± 0.1, and 1.2 ± 0.2 nm, respectively, and those of the films using the TDMAH precursor were 1.5 ± 0.1, 1.4 ± 0.1, and 1.9 ± 0.1 nm, respectively. This shows that oxygen diffusion through the HfO_2 layer grown from BTEMAH is much less active than the HfO_2 layer grown from TDMAH. This can be explained by the difference in Hf density and crystallinity. The interfacial layer thickness from BTEMAH is almost invariant up to 700 °C, which suggests that the amorphous-structured upper layer works as a good diffusion barrier for oxygen. However, after annealing at 1000 °C, the film is totally crystallized and the interfacial layer thickness increases slightly through enhanced oxygen diffusion probably along the grain boundaries. For the films grown from TDMAH, the upper layer thickness decreased during high temperature annealing due to the densification effect. This also suggests that the as-grown film from TDMAH has a lower Hf density than that of the film grown from BTEMAH, as shown in Fig. 5. The upper layer of the film from TDMAH, which has a low Hf density, shrinks when it transforms to a stable crystalline structure. Fine cracks and defects can be generated as a result of this sudden shrinkage, which creates more diffusion paths in the film. Therefore, the interfacial layer thickness increases abruptly at 1000 °C due to the complete crystallization and enhanced diffusion of oxygen through the less dense and thin crystalline layer. All these structural changes have a significant influence on the electrical properties of the films.

Electrical properties

The electrical properties of HfO_2 films were investigated with a capacitor structure of Pt (100 nm)/HfO_2/Si substrate. In general, the dielectric properties of high-k films are compared using the capacitance equivalent thickness (CET), which is the thickness of SiO_2 required to obtain an equivalent capacitance (C_m) measured from a high-k dielectric capacitor. Therefore, the CET can be determined using a simple equation: $CET = A\varepsilon_o k_{ox}/C_m$, where A is the top electrode area, ε_o is the permittivity of a vacuum and k_{ox} is the dielectric constant (3.9) of SiO_2. This is because from the definition of the CET, $C_m = A\varepsilon_o k_{HfO2}/t_{HfO2} = A\varepsilon_o k_{ox}/CET$, where k_{HfO2} and t_{HfO2} are the dielectric constant and physical thickness of the HfO_2, respectively.

In Fig. 9, the CET values of the HfO_2 films were obtained from the accumulation capacitances of the capacitance–voltage curves. The leakage currents in the accumulation region were not so high as to adversely affect the measurement of the accumulation capacitances. Fig. 9(a), (b), and (c) show changes in the CET of HfO_2 films grown from BTEMAH and TDMAH as a function of the film thickness for the as-grown films and films annealed at 700 and 1000 °C, respectively. Fig. 9(d) shows the C–V curves of the film annealed at 700 °C using BTEMAH and TDMAH precursors, respectively. Here, the films were deposited by 53 cycles. There is negligible hysteresis in the C–V of the film using BTEMAH, which suggests that charge trapping is minimized, whereas the hysteresis of the film using TDMAH was ~50 mV. The flat band voltage of the HfO_2 film using TDMAH was shifted into the positive voltage direction compared with that of the film using BTEMAH, which suggests that the film has a higher negative fixed charge density.

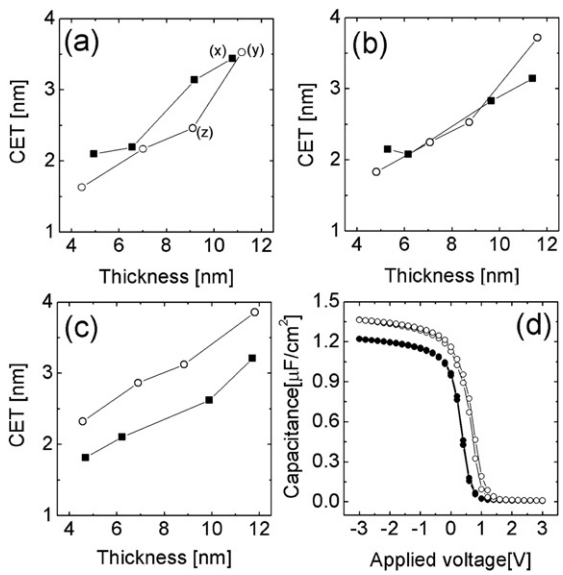

Fig. 9 Changes in the CET of (a) as-grown, (b) 700 °C annealed, and (c) 1000 °C annealed HfO_2 films using BTEMAH (closed circles) and TDMAH (open circles), respectively, as a function of the film thickness. (d) C–V curves of the HfO_2 films annealed at 700 °C using BTEMAH (closed circles) and TDMAH (open circle). Labels (x), (y) and (z) in (a) denote the thickest film using BTEMAH, the thickest film using TDMAH, and the 8.4 nm-thick film using TDMAH, respectively.

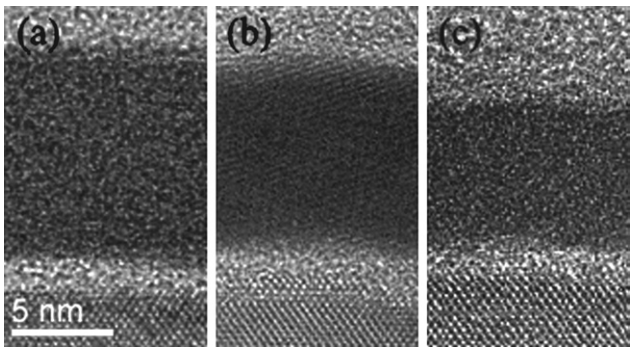

Fig. 10 HRTEM cross-section images of the as-deposited HfO_2 films using (a) BTEMAH (10.8 nm), (b) TDMAH (11.2 nm) and (c) TDMAH (9.1 nm). The CET values of these films correspond to points (x), (y) and (z) in Fig. 9(a), respectively.

If the interfacial layer thickness is assumed to be constant with the total film thickness under the given annealing conditions, the inverse slope of the linear fit of each graph in Fig. 9(a–c) should correspond to the dielectric constant (k) of the upper layer. However, the CET variation with the total film thickness is not linear over the entire film thickness range. However, the distinctive points from the linear slope suggest that the films have different structures at different thicknesses depending on the annealing conditions. The thinnest as-grown film from BTEMAH shows an unexpectedly large CET value so that it deviates from the linear trend (Fig. 9(a)). This might be due to the high proportion of the interfacial layer in the film. In Fig. 9(b), the point of this thinnest film is more distinguishable from the trend of the other points because the film remained amorphous after annealing at 700 °C while the others crystallized and densified. The film finally crystallized after annealing at 1000 °C. Hence, its CET decreased due to densification and followed the trend. This agrees well with the HRTEM images of the thin HfO_2 films using BTEMAH in Fig. 8(a)–(c). Among the as-grown films using TDMAH, the thickest film had a crystalline upper layer in the as-deposited state. Therefore, it also deviates from the linear trend (Fig. 9(a)). The crystalline upper layer induces more serious Si and O diffusion along the grain boundaries so that the CET of this film is higher than that expected from the linear trend. Indeed, the HRTEM images in Fig. 10 confirmed that the thickest film using TDMAH (point (y)) is the only one that crystallized in the as-deposited state among the films shown in Fig. 9(a). Fig. 10(a) shows a HRTEM image of a 10.8 nm-thick as-grown film from BTEMAH, which corresponds to point (x) shown in Fig. 9(a). Fig. 10(b) and (c) show images of 11.2 and 9.1 nm-thick as-grown films from TDMAH, which correspond to points (y) and (z), respectively, in Fig. 9(a). The 8.6 nm-thick film from TDMAH (point (z)) is still amorphous but the thickest film (point (y)) became crystalline and its interfacial layer increased. In contrast, the upper layer of the as-grown film (point (x)) from BTEMAH was amorphous and its interfacial layer was relatively thin despite its thickness being similar to that of the thickest film from TDMAH (point (y)). Therefore, the increase in interfacial layer thickness during crystallization makes the largest contribution to the rapid increase in the CET of the as-grown film (point (y)) from TDMAH. After annealing at 1000 °C, all the films had a crystalline structure, and linear trends were observed in the whole thickness region for the two film types. The calculated k values of the fully crystallized HfO_2 films from BTEMAH and TDMAH were ~21 and ~19, respectively, after 1000 °C annealing. The slopes of the two films showed similar k values but the y-axis intercept of the films from TDMAH was much higher than that of the films from BTEMAH, as in Fig. 9(c). This suggests that the interfacial layer of the films from TDMAH increased seriously due to Si and O diffusion after high temperature annealing.

A general trend in the whole film thickness range can be described despite some of outlying points in the CET *vs.* thickness graphs. The CET values of the as-grown films from BTEMAH are generally larger than those of the as-grown films from TDMAH in the whole film thickness region in Fig. 9(a). However, the trend reversed after annealing, particularly after annealing at 1000 °C. The CET of the annealed films grown with TDMAH were much larger than those of the annealed films grown with BTEMAH over the whole thickness range. In the case of the films grown with BTEMAH, the amorphous structure suppresses the diffusion of O and Si effectively and the high Hf density prevents shrinkage of the upper layer of the film during crystallization. As a result, the films grown with BTEMAH have better thermal stability, which is a crucial merit of the BTEMAH precursor.

The denser and more amorphous-like nature of the films grown from BTEMAH also improves the leakage current properties. Fig. 11(a), (b), and (c) show the J–V curves of the as-grown films (corresponding to points (x) and (y) in Fig. 9(a)), as well as the J–V curves of the films annealed at 700 and 1000 °C. The J value of the as-grown film from BTEMAH was

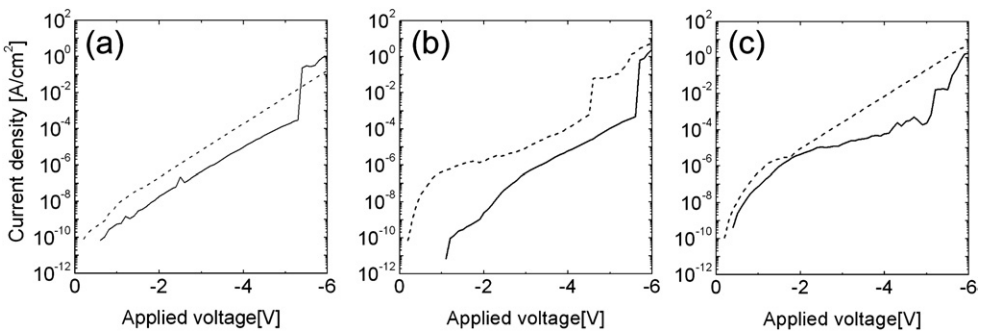

Fig. 11 Leakage current densities of the HfO_2 films using BTEMAH at point (x) (—) (in Fig. 9(a)) and using TDMAH at point (y) (- - -) (in Fig. 9(a)); (a) as-deposited, and annealed at (b) 700 °C, and at (c) 1000 °C.

10 times lower than that of the as-grown film from TDMAH. The difference was maintained even after annealing. Although the data are not shown, the thinner films showed an even larger difference. It should be noted that the flat band voltage of the film using TDMAH was higher (more positive) than that of the film using BTEMAH (Fig. 9(d)). Hence, a correction of the applied voltage using the flat band voltage shift induces an even larger difference in leakage current between the two films. More detailed information on the leakage conduction behavior of the films grown from BTEMAH will be reported elsewhere.

Conclusions

A new heteroleptic hafnium precursor of *tert*-butoxy-tris(ethylmethylamido)hafnium [$HfO^tBu(NEtMe)_3$; BTEMAH] and ozone were used to grow HfO_2 thin films on Si substrates by ALD. The growth behavior and various structural, chemical, and electrical properties of the films were compared with those of the films grown from another hafnium precursor of tetrakis(dimethylamido)hafnium (TDMAH). The use of BTEMAH resulted in the highest growth rate of 0.16 nm $cycle^{-1}$ among those reported for HfO_2 ALD, which is a crucial merit of this precursor. The HfO_2 films deposited using BTEMAH also showed almost 20% improvement in the Hf density in the films compared with the films grown from TDMAH. In addition, the as-grown films from BTEMAH maintained an amorphous structure up to a thickness of ~15 nm due to the higher density. They also showed enhanced resistance to crystallization during annealing up to 800 °C, which resulted in excellent thermal stability of the dielectric performance. The CET values of the films with thicknesses ranging from 4 to 13 nm showed a negligible increase up to 1000 °C. To our knowledge, this level of thermal stability has not been reported for a single HfO_2 layer. All these improvements in the growth behavior and electrical performance of the HfO_2 films were attributed to the heteroleptic hafnium precursor, BTEMAH.

Acknowledgements

The work was supported by the system IC 2010 project of the Korean government.

References

1 T. Suntola, *Mater. Sci. Rep.*, 1989, **4**, 261.
2 M. Leskelä and M Ritala, *Thin Solid Films*, 2002, **409**, 138.
3 M. A. Cameron, I. P. Gartland, J. A. Smith, S. F. Diaz and S. M. George, *Langmuir*, 2000, **16**, 7435.
4 A. Nakajima, T. Kidera, H. Ishii and S. Yokoyama, *Appl. Phys. Lett.*, 2002, **81**, 2824.
5 M. Cho, J. Park, H. B. Park and C. S. Hwang, *Appl. Phys. Lett.*, 2002, **81**, 334.
6 L. Nyns, L. Hall, T. Conard, A. Delabie, W. Deweerd, M. Heyns, S. V. Elshocht, N. V. Hoornick, C. Vinckier and S. D. Gendt, *J. Electrochem. Soc.*, 2006, **153**(9), F205.
7 P. D. Kirsch, M. A. Quevedo-Lopez, H. -J. Li, Y. Senzaki, J. J. Peterson, S. C. Song, S. A. Krishnan, N. Moumen, J. Barnett, G. Bersuker, P. Y. Hung and B. H. Lee, *J. Appl. Phys.*, 2006, **99**, 023508.
8 K. Kukli, M. Ritala and M. Leskelä, *Chem. Vap. Deposition*, 2000, **6**, 297.
9 D. M. Hausmann, E. Kim, J. Becker and R. G. Gordon, *Chem. Mater.*, 2002, **14**, 4350.
10 X. Liu, S. Ramanathan, A. Longdergan, A. Srivastava, E. Lee, T. E. Seidel, J. T. Barton, D. Pang and R. G. Gordon, *J. Electrochem. Soc.*, 2005, **152**(3), G213.
11 K. Kukli, M. Ritala, T. Sajavaara, J. Keinonen and M. Leskelä, *Chem. Vap. Deposition*, 2002, **8**(5), 199.
12 A. Soulet, L. Duquesne, G. Jursich, R. Inman, A. Misra, N. Blasco, C. Lachaud, Y. Marot, R. Prunier, M. Vautier, S. Anderson, P. Clancy and M. Havlicek, *Semiconductor Fabtech*, 2005, 27th edition, 10/5.
13 J. Niinistö, M Putkonen, L. Niinistö, F. Song, P. Williams, P. N. Heys and R. Odedra, *Chem. Mater.*, 2007, **19**, 3319.
14 M. Cho, H. B. Park, J. Park, S. W. Lee and C. S. Hwang, *Appl. Phys. Lett.*, 2003, **83**, 5503.
15 H. B. Park, M. Cho, J. Park, S. W. Lee, C. S. Hwang, J.-P. Kim, J.-H. Lee, N.-I. Lee, H.-K. Kang, J.-C. Lee and S.-J. Oh, *J. Appl. Phys.*, 2003, **94**, 3641.
16 M. Cho, D. S. Jeong, J. Park, H. B. Park, S. W. Lee, T. J. Park and C. S. Hwang, *Appl. Phys. Lett.*, 2004, **85**, 5953.
17 Y.-G. Park, J.-H. Yeo, E.-A. Chung, K.-V. Im, Y.-S. Kim, S.-T. Kim and C.-Y. Yoo, US Pat., 2006, 0205198.
18 Y. F. Loo, R. O'Kane, A. C. Jones, H. C. Aspinall, R. J. Potter, P. R. Chalker, J. F. Bickley, S. Taylor and L. M. Smith, *J. Mater. Chem.*, 2005, **15**, 1896.
19 K. Kukli, M. Ritala, M. Leskelä, T. Sajavaara, J. Keinonen, A. C. Jones and J. L. Roberts, *Chem. Vap. Deposition*, 2003, **9**(6), 315.
20 J. Park, M. Cho, S. K. Kim, T. J. Park, S. W. Lee, S. H. Hong and C. S. Hwang, *Appl. Phys. Lett.*, 2005, **86**, 112907.
21 S. Kamiyama, T. Miura and Y. Nara, *Electrochem. Solid-State Lett.*, 2006, **9**(9), G285.
22 T. Watanabe, S. Hoffmann-Eifert, C. S. Hwang and R. Waser, *J. Electrochem. Soc.*, 2006, **153**(9), F199.
23 T. Watanabe, S. Hoffmann-Eifert, L. Yang, A. Rüdiger, C. Kügeler, C. S. Hwang and R. Waser, *J. Electrochem. Soc.*, 2007, **154**(6), G134.
24 D. R. Lide, *Handbook of Chemistry and Physics 75th edition*, CRC Press, Boca Raton, FL, 1994.
25 S. Consiglio, F. Papadatos, S. Naczas, S. Skordas, E. T. Eisenbraun and A. E. Kaloyeros, *J. Electrochem. Soc.*, 2006, **153**(11), F249.